Research Article

Shunt Active Power Filter Based on Proportional Integral and Multi Vector Resonant Controllers for Compensating Nonlinear Loads

Sen Ye [ID],[1] **Youbing Zhang** [ID],[1] **Luyao Xie** [ID],[1] and **Haiqiang Lu**[2]

[1]*College of Information Engineering, Zhejiang University of Technology, Hangzhou, China*
[2]*Jiaxing Heng Chuang Electric Equipment Co., Ltd., Jiaxing, China*

Correspondence should be addressed to Luyao Xie; xieluyao@zjut.edu.cn

The current tracking control strategy determines the compensation performance of shunt active power filter (SAPF). Due to inadequate compensation of the main harmonic by traditional proportional integral (PI) control, a control algorithm based on PI and multi vector resonant (VR) controllers is proposed to control SAPF. The mathematical model of SAPF is built, and basic principle of VR controller is introduced. Under the synchronous reference frame, the proposed control method based on pole zero cancellation is designed, which narrows the order of the control system and improves the system dynamic response and the control accuracy. Then the feasibility of the method is demonstrated by analyzing the closed loop frequency characteristics of the system. Finally, the simulation and experimental results are carried out to verify the performance of the proposed method.

1. Introduction

In recent years, with the intensification of the global energy crisis, the renewable energy and power electric technology have been integrated, which has promoted the development of distributed generators (DGs) [1, 2]. The speed driver of small motor, voltage source converter, and a large number of nonlinear loads including electric arc furnace, high-power rectifier, transducer, and fluorescent are connected to the grid, which will cause harmonic pollution unavoidably [3–5]. The power grid operates in this state for a long run, which will bring great harm to power system and power consumers, mainly manifested in the following respects: (1) The line loss of the system is increasing greatly, and the operating efficiency of the grid is reduced. A lot of 3rd harmonics will also increase the neutral current, leading to the damage of the custom power devices. (2) It makes the motor vibrate and produce noise, which affects the safety operation in production. (3) It makes the relay protection device act by mistake, which interrupts the power supply and makes the extent loss to production. (4) It interferes with measuring instruments and communication systems [6–8].

Therefore, it is urgent to control the power harmonic pollution to improve the power quality.

As a new type of power electronic device that can suppress harmonics dynamically, a three-phase three-wire SAPF with excellent performance has been widely used in the field of power quality. The real-time and accurate compensation for the fast changing harmonic currents is an important guarantee for the operation of SAPF safely and reliably. In the past years, a lot of research and analysis have been done on the detection and tracking control strategy of the harmonic currents. In [9, 10], it transforms the harmonic component to the DC component through multisynchronous rotating coordinate transformation; thus, traditional PI controller can be utilized to track the harmonics with zero steady-state error; however, it is too complicated. The hysteresis current control method presented in [11, 12] with quickly dynamic respond performance is simple and easy to realize without carrier modulation, but the control accuracy is inversely proportional to switching frequency. In addition, the switching frequency is not fixed, which sets a higher request to switching device. In [13, 14], the repetitive control theory was developed to solve harmonic problems, which has the advantages of good

robustness, simple structure, and easy implementation. However, dynamic performance is limited if the load changes suddenly. In order to overcome the effect of computational delay and control delay on compensation performance, the dead-beat control in [15, 16] is used to track the reference current, which plays a certain effect, but it highly depends on the system parameters. When the system parameters change, the compensation performance will be greatly affected. In [17, 18], vector resonant(VR) control method is proposed, where proportional controller is to adjust the control bandwidth to improve the dynamic response speed, while the resonant controller is to select frequency for specific frequency signal to improve the control accuracy of current. However, it can not compensate the phase delay of controlled object.

Viewing of the shortcomings of above methods, a current control method based on PI and VR controller is proposed to compensate the selected harmonics accurately. The proportional control can improve the dynamic performance of the current loop and the fundamental current. The VR controller can control a group of positive and negative sequence harmonic currents with zero steady-state error by the idea of zero pole cancellation. Finally, the feasibility and validity of the proposed strategy are confirmed by simulation based on Matlab/Simulink and a prototype of the SAPF using TMS320F28335 as control core.

2. Modeling of SAPF

The structure of two-level three-phase three-wire SAPF used in this paper is shown in Figure 1 [19]. The mathematical model can be described in three-phase ABC static coordinate system as follows:

$$L\frac{di_{Fa}}{dt} + Ri_{Fa} = u_a - e_{Sa},$$

$$L\frac{di_{Fb}}{dt} + Ri_{Fb} = u_b - e_{Sb}, \qquad (1)$$

$$L\frac{di_{Fc}}{dt} + Ri_{Fc} = u_c - e_{Sc},$$

where e_a, e_b, and e_c are the 3-phase source voltage; u_a, u_b, and u_c are the 3-phase output voltage of SAPF; i_{sa}, i_{sb}, and i_{sc} are source current; i_{Fa}, i_{Fb}, and i_{Fc} are the compensation currents of SAPF; $S_a - S_c^*$ are fully controlled switch devices; L is AC-link inductance; C is DC-link capacitance; u_{dc} is DC-link voltage; and R is the equivalent loss of the AC-link inductance and switch device.

By means of Clarke transform and Park transform, the mathematical model under the synchronous reference frame is given as follows:

$$L\frac{di_{Fd}}{dt} + Ri_{Fd} = u_d + \omega_s L i_{Fq} - e_{Sd},$$

$$L\frac{di_{Fq}}{dt} + Ri_{Fq} = u_q - \omega_s L i_{Fd} - e_{Sq}. \qquad (2)$$

$e_d, e_q u_d, u_q$ and i_{Fd}, i_{Fq} are d-axis components and q-axis components of the three-phase source voltage, AC-link output voltage, and compensation current of the SAPF
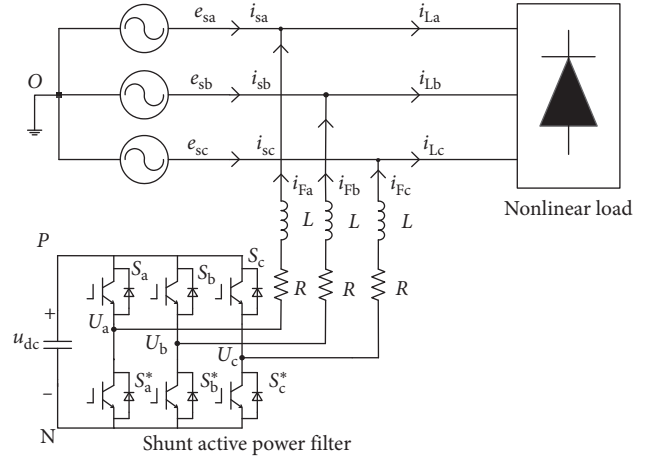

FIGURE 1: Structure of three-phase three-wire SAPF.

under synchronous reference frame, respectively. ω_s represents the voltage angle frequency detected by a software phase-locked loop.

3. Basic Principle of VR Controller

The current controller based on VR control has a higher gain at its resonant frequency, which can control the AC current at the resonant frequency with high precision. The transfer function of the VR controller can be derived as [20]

$$G_{VRh}(s) = \frac{K_{ph}s^2 + K_{ih}s}{s^2 + (h\omega_s)^2}, \qquad (3)$$

where K_{ph} and K_{ih} are proportional coefficient and the integral coefficient, respectively, and $h\omega_s$ is the resonant angle frequency. The absolute value of h represents the order of the harmonic currents, the sign of which represents the rotation direction in sequence component diagram. When h is positive, it represents that harmonic currents are in positive sequence. Otherwise, it represents that harmonic currents are in negative sequence.

The bode diagram of VR controller is shown in Figure 2 for $K_{ph} = 1, K_{ih} = 50, h = 6, \omega_s = 100\pi$. On one hand, the open loop gain of VR controller is infinity at its two resonant points $\pm h\omega_s$, but for other frequencies, the gain is rapidly attenuated. On the contrary, the VR controller is phase-leading about 180° at the frequency of $0 \sim h\omega_s$. Once the angular frequency exceeds the resonant frequency, the phase jumps from 180° to 0°. But at negative frequency, it appears on the opposite performance. On the basis of the analysis above, it shows that VR controller has a good control precision for the signal at the resonant frequency.

4. Current Control Strategy of SAPF

4.1. VR Controller for Compensating Harmonic Currents. For the three-phase uncontrollable rectifier, the main harmonic currents consist of 5th of negative sequence, 7th of positive sequence, 11th of negative sequence, 13th of positive
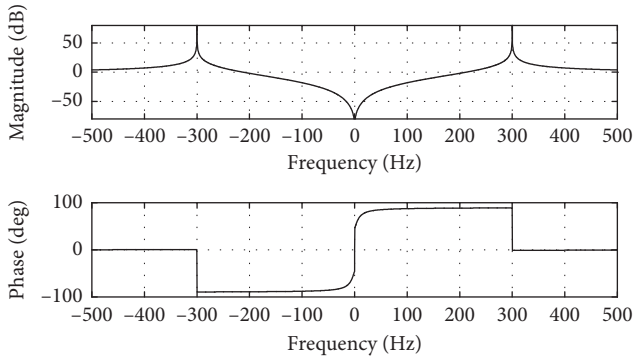
Figure 2: Bode diagram of VR controller.

Figure 3: Current control block diagram based on multi-VR controller.

Figure 4: Bode diagram of harmonic current close loop control.

harmonic, and so on, such that $h = \pm 6n + 1, n$ is $1, 2, \ldots$. Since the synchronous reference frame provides a frequency shift of -50 Hz, the main harmonic current in fundamental frame transforms to 6th of positive and negative sequence harmonic, 12th of positive and negative sequence harmonic, and so on. The harmonic orders become $h = \pm 6n$. Thus the multi-VR controller can compensate the selected harmonic based on formula (3). The equivalent gain of the SAPF K_{PWM} is set to 1. The current control block diagram is shown in Figure 3, where $P(s) = 1/(Ls + R)$ is the transfer function of the controlled object.

Taking the d-axis current as an example, current open loop transfer function of the multi-VR controller is

$$G_{\mathrm{o}}(s) = \sum_{h=6n,n=1,2}^{5} G_{\mathrm{VR}h}(s)P(s)$$
$$= \sum_{h=6n,n=1,2}^{5} \frac{K_{\mathrm{p}h}s^2 + K_{\mathrm{i}h}s}{\left(s^2 + (h\omega_s)^2\right)(Ls + R)}. \tag{4}$$

The basic idea of VR control is to adopt the zero point of the control to offset the poles of the controlled object, so as to compensate for the phase lag of the controlled object, thus improve the control accuracy of the harmonic currents. The zero of the controller can effectively cancel the poles of the controlled object on condition that $K_{\mathrm{p}h} = K_{\mathrm{i}h} * L/R$, and the simplified open loop transfer function is given as

$$G_{\mathrm{o}}(s) = \sum_{h=6n,n=1,2}^{5} \frac{K_{\mathrm{p}h}s}{L\left(s^2 + (h\omega_s)^2\right)}. \tag{5}$$

The closed loop transfer function is

$$G_{\mathrm{c}}(s) = \frac{G_{\mathrm{o}}(s)}{1 + G_{\mathrm{o}}(s)} = \frac{\sum_{h=6n,n=1,2}^{5}\left(K_{\mathrm{p}h}s/L\left(s^2 + (h\omega_s)^2\right)\right)}{1 + \sum_{h=6n,n=1,2}^{5}\left(K_{\mathrm{p}h}s/L\left(s^2 + (h\omega_s)^2\right)\right)}. \tag{6}$$

The values of $K_{\mathrm{p}h}, K_{\mathrm{i}h}, L,$ and R in formulae (4)–(6) are both greater than 0. The bode diagram of harmonic current close loop control is depicted in Figure 4, at the resonant frequency, the amplitude gain of the transfer function is 1 without phase delay, which indicates that the VR controller has frequency selection function on a pair of harmonic currents and can be controlled with zero steady-state error.
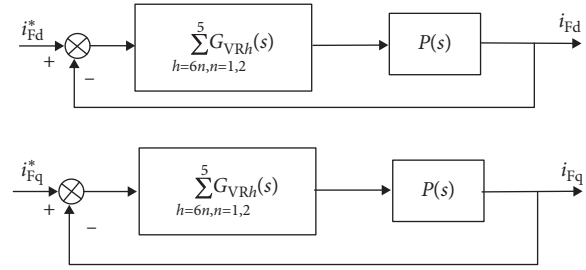
Therefore, the system is stable even when the circuit parameters and VR parameters change.

Whether SAPF can operate stably is affected not only by its own system parameters, but also by external disturbances, and the grid voltage is the most important factor for SAPF. Next, the tracking performance of compensation current is analyzed, when the grid voltage is disturbed. The current control block is shown in Figure 5.

When controlling any order of harmonic, the transfer function of compensation current caused by grid voltage disturbance is

$$\Phi_{\mathrm{en}}(s) = \frac{P(s)}{1 + G_0(s)} = \frac{1}{(Ls + R)\left(1 + \left(K_{\mathrm{p}h}s/L\left(s^2 + (h\omega_s)^2\right)\right)\right)}. \tag{7}$$

At the resonant frequency, the amplitude gain caused by the grid voltage disturbance tends to 0, that is, the steady-state error is 0, which indicates that the compensation current is affected by the voltage disturbance very little by using the VR controller.

4.2. PI Controller for Compensating Fundamental Current. The previous section demonstrates that the VR controller with double resonant frequency can compensate the harmonic with zero steady-state error, but from bode diagram of harmonic close loop control, the amplitude gain of the current near 0 Hz is very small, which means that the VR
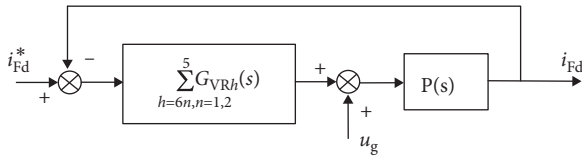
Figure 5: Current control block diagram when the system is disturbed by the grid voltage.

Figure 6: Fundamental current control block diagram based on PI controller.

Figure 7: Bode diagram of fundamental close loop control.

controller is not ideal for the low frequency signal including DC current signal and has the problem of slow dynamic response. However, in addition to controlling the harmonic currents, the SAPF needs to control the fundamental current from voltage controller to compensate for its loss. The DC current obtained fundamental current by the synchronous reference frame. So, it is necessary to ameliorate the VR controller to improve the gain of the low frequency signals. For $h = 0$ in formula (3), the VR controller can be transformed to PI controller, as shown in the following formula:

$$G_{PI}(s) = \frac{K_{p0}s + K_{i0}}{s}. \tag{8}$$

The fundamental current control block diagram based on PI controller is given in Figure 6.

The fundamental current closed loop transfer function based on the PI controller is

$$\Phi_c(s) = \frac{K_{p0}s + K_{i0}}{Ls^2 + (R + K_{p0})s + K_{i0}}. \tag{9}$$

For $K_{p0}/K_{i0} = L/R$, the zero point of the PI controller is used to offset the pole of the controlled object; thus, the phase delay of the controlled object is compensated. That is,

$$\Phi_c(s) = \frac{K_{p0}}{Ls + K_{p0}}. \tag{10}$$

The closed loop transfer function shown in formula (10) is a typical first-order inertia link, and its control bandwidth is $\omega = K_{p0}/L$; that is, the cut-off frequency of the transfer function is $f_c = K_{p0}/2\pi L$. When L is constant, the bigger K_{p0} is, the bigger bandwidth ω is, which represents that the response speed of current loop is faster; when K_{p0} is constant, the bigger L is, the bigger bandwidth ω is, which represents that the response speed of current loop is slower.

The bode diagram of fundamental close loop control is given in Figure 7 for $L = 3$ mH and $K_{p0} = 1, 10, 20$. At the frequency of 0 Hz, the amplitude gain of the fundamental current is 1 without phase delay. However, the gain is rapidly attenuated outside 0 Hz. It indicates that the PI controller has the function of frequency selection for the DC current under the synchronous reference frame, which can achieve high precision control.

4.3. The Influence of Digital Control Delay. Digital control delay, including computation delay and PWM update link delay, will affect tracking performance of the current loop and even cause instability of the system. Thus, it is necessary to study the effect of control delay on the tracking performance of the current loop. The delay of the digital control is
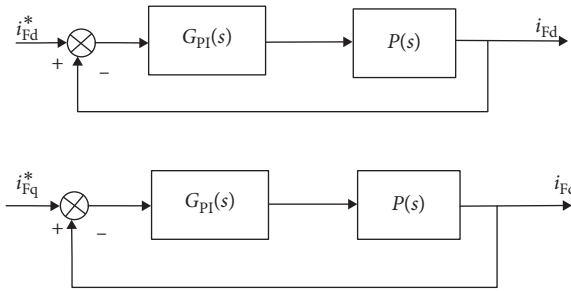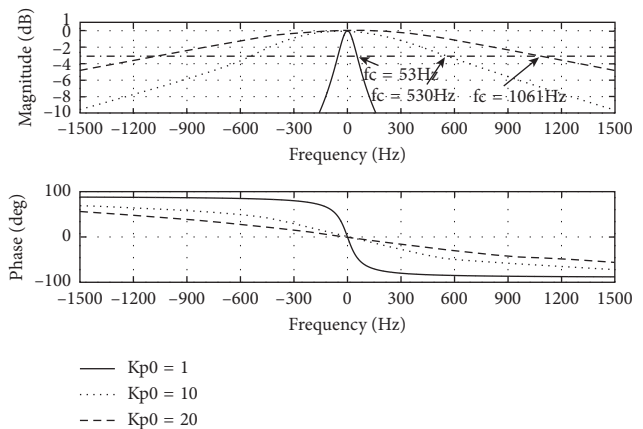
generally 1.5 times of the sample period T_s [21], and the transfer function can be expressed as

$$G_d(s) = \frac{1}{1.5T_s * s + 1},$$

$$G_c(s) = \frac{\sum_{h=6n,n=1,2}^{5}\left(K_{ph}s/L\left(s^2 + (h\omega_s)^2\right)(1.5T_ss + 1)\right)}{1 + \sum_{h=6n,n=1,2}^{5}\left(K_{ph}s/L\left(s^2 + (h\omega_s)^2\right)(1.5T_ss + 1)\right)}. \tag{11}$$

Bode diagram of closed loop current considering digital control delay is shown in Figure 8 for $L = 3$mH, $T_s = 10^{-4}$ s, $K_{ph} = 0.4$. Even if affected by the digital control delay, the current loop has 35° of phase margin, which is still stable. In addition, the phase shift is still 0 at every positive and negative sequence harmonic frequency, which indicates that the digital control delay has less influence on the system and the current loop still has high static control accuracy.

4.4. Design of Control System. The control block diagram of the three-phase three-wire SAPF for the proposed method is shown in Figure 9. The PI control is used to maintain DC-link voltage stability in the external voltage loop. The difference between the reference voltage u_{dc}^* and the actual voltage u_{dc} is input to the PI controller and the output of PI controller as a part of active power loss is added to the active source current component. PI and VR control is used in the internal current loop. The harmonic currents i_{hd}^* and i_{hq}^*
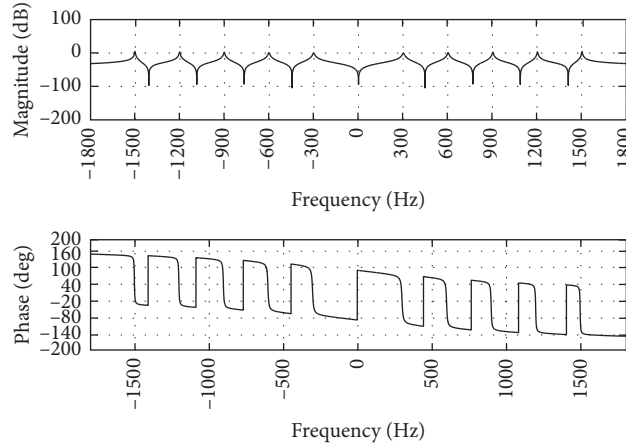
Figure 8: Bode diagram of closed loop current considering digital control delay.
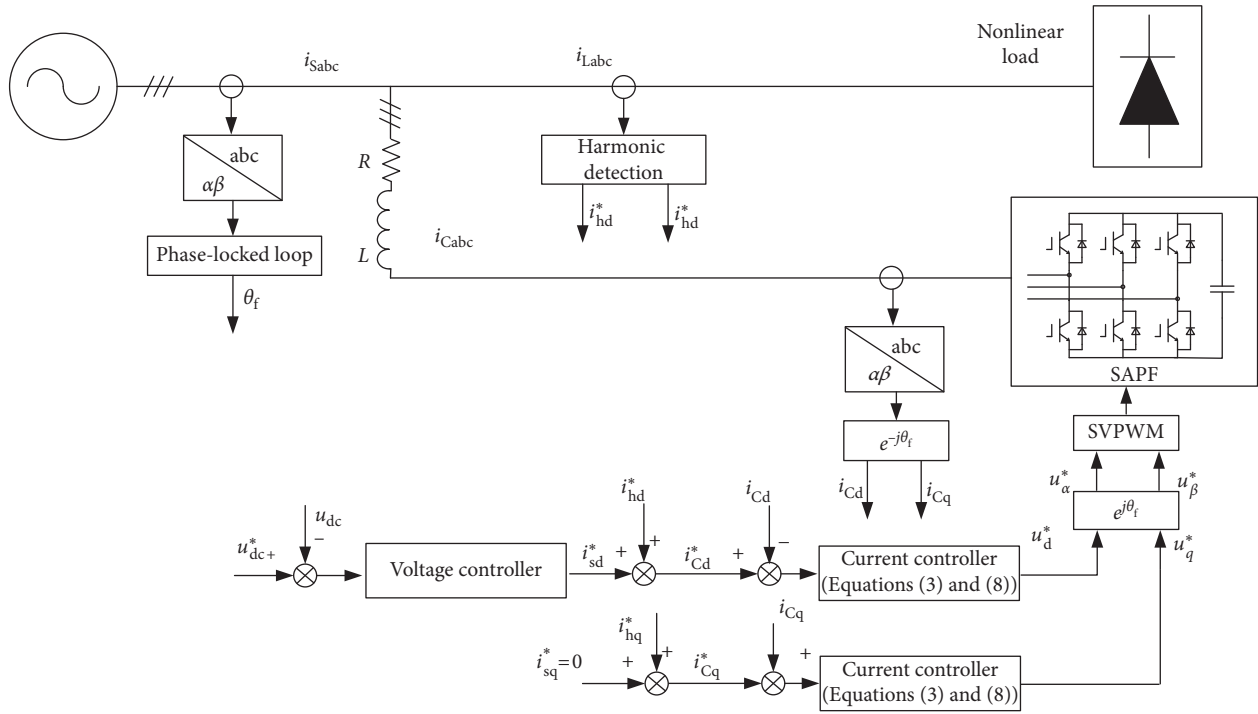

Figure 9: Control block diagram of three-phase three-wire SAPF.

extracted from the load current i_{Labc} by instantaneous reactive power theory is added to the output of the PI controller i_{sd}^* and i_{sq}^*. Compensation current i_{Cabc} is turned to i_{cd} and i_{cq} based on synchronous coordinate transformation; then the difference between i_{cd}, i_{cq} and i_{cd}^*, i_{cq}^* is input to the current controller; besides, the control pulse signal required by SAPF is obtained by the space vector pulse width modulation (SVPWM) to compensate the harmonic currents [22].

5. Simulation and Experimental Results

In order to verify the correctness and effectiveness of the proposed current control method based on PI and multi-VR control in this paper, both classical PI controller and PI + multi-VR controller are designed according to the above-mentioned

Table 1: Simulation model parameters.

Parameter	Value
Source voltage V_{snom}	220 V, 50 Hz
DC-link voltage V_{dcref}	750 V
DC-link capacitance C	1000 μF
Filter inductance L_f	3 mH
Equivalent loss resistance R_f	0.3 Ω
Nonlinear load	Three-phase diode bridge rectifier with a 10 Ω DC resistor

method in Matlab/Simulink. The simulation model parameters are shown in Table 1.

Since both of the power supply and the nonlinear load are three-phase symmetry, the A phase is only analyzed in
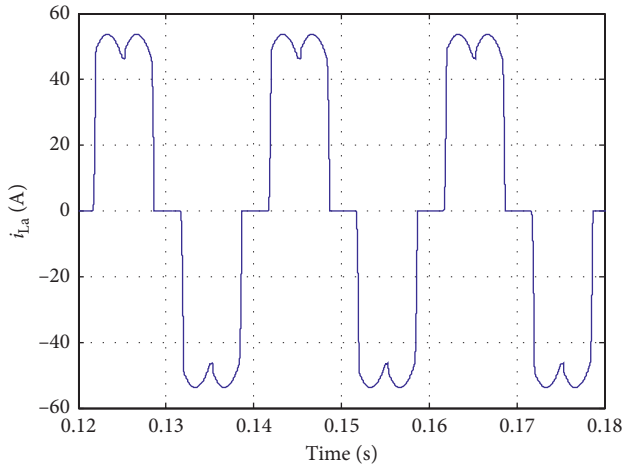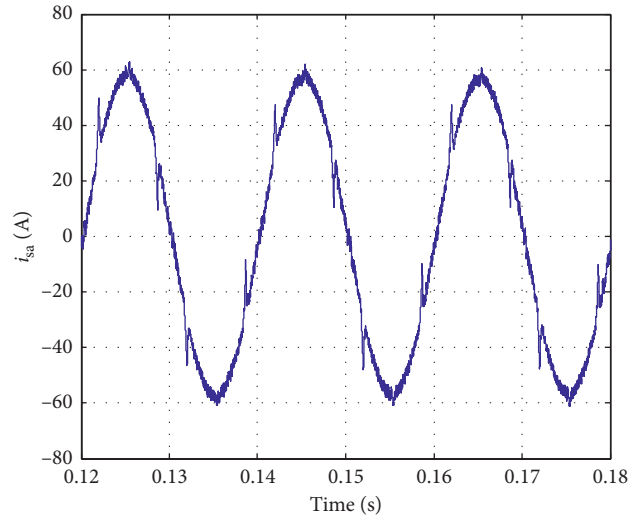
Figure 10: Waveform of nonlinear load current.
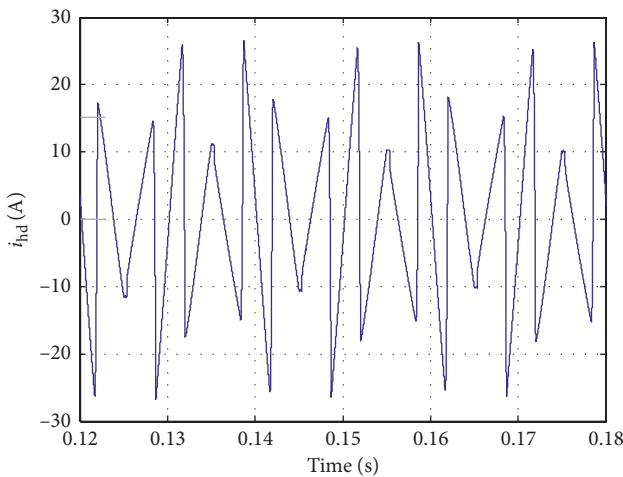

Figure 11: Waveform of harmonic currents.

Figure 12: FFT analysis of nonlinear load current.

Figure 13: Waveform of source current using PI controller.

Fundamental (50 Hz) = 56.82, THD = 7.37%

Figure 14: FFT analysis of source current using PI controller.

the simulation waveform. The waveform of the load current and harmonic currents are depicted in Figures 10 and 11, and the FFT analysis of the nonlinear load current are shown in Figure 12. From Figure 11, the total harmonic distortion (THD) before compensation is up to 28.92%, and the load current's harmonic spectrum contains harmonics of the order $h = 6n \pm 1, n = 1, 2, \ldots$.

The compensation performance using PI controller is shown in Figures 13 and 14, respectively. The compensation results of the proposed control strategy based on PI and 6th VR controller are shown in Figures 15 and 16, respectively. Comparing the four figures, PI controller can compensate a part of harmonic, which is not too fruitful. After adopting the 6th of the VR controller, the 5th harmonic and 7th harmonic can be compensated effectively. 5th harmonic is reduced to 0.28% from 2.08%. 7th harmonic is reduced to
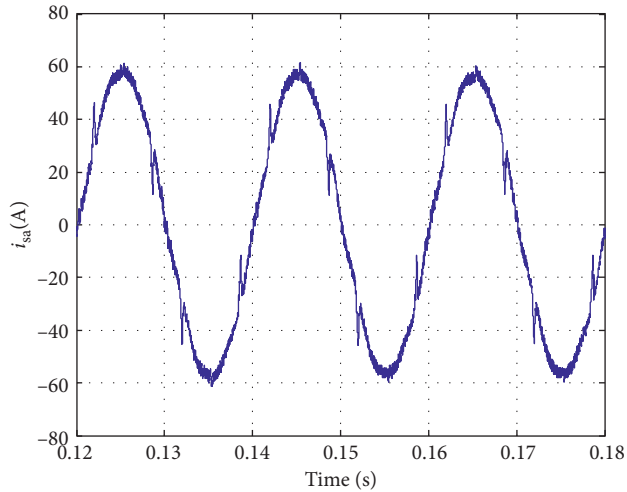
Figure 15: Waveform of source current using PI controller and 6th VR controller.
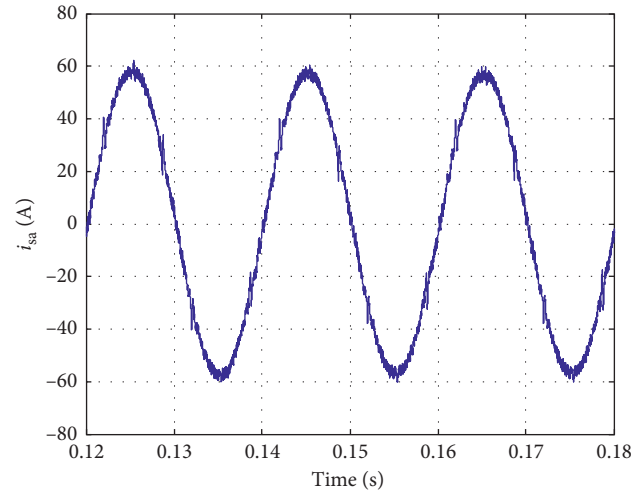

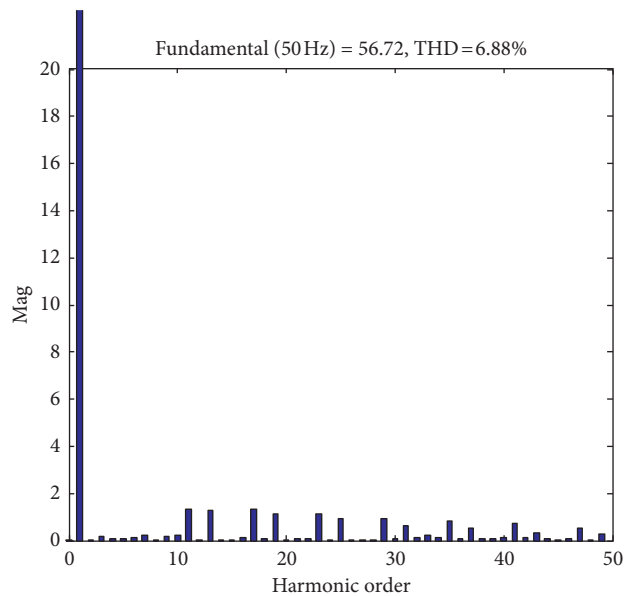Figure 17: Waveform of source current using PI controller and multi-VR controllers.

Figure 16: FFT analysis of nonlinear load current using PI controller and 6th VR controller.
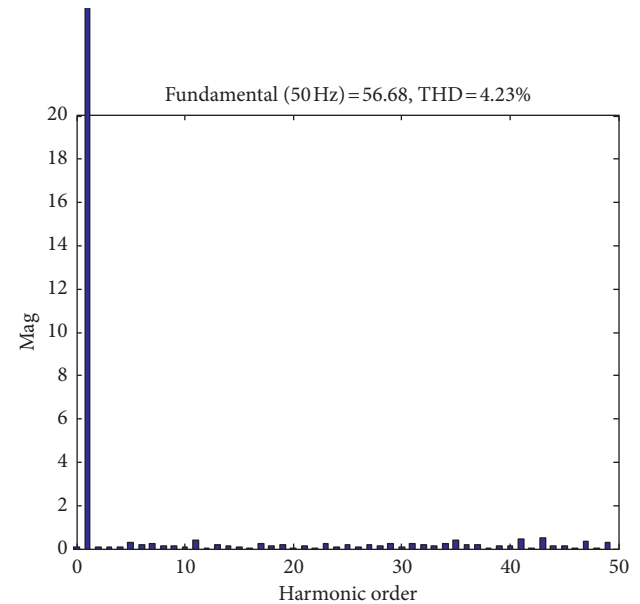

Figure 18: FFT analysis of nonlinear load current using PI controller and multi-VR controllers.

0.11% from 2.16%, but distortion rate of other harmonics remains the same. The simulation results show that the 6th resonant controller has good inhibitory effects on 5th harmonic and 7th harmonic, which can further improve the compensation performance for some specific harmonics.

The compensation results using PI controller and multi-VR controller are shown in Figures 17 and 18. When the PI and multi-VR controllers are introduced in the control system, distortion rate of each harmonic decreases remarkably.

The experimental waveforms based on PI + multi-VR controllers proposed in the case of abrupt loading is shown in Figure 19. It is known from Figure 19 that at 0.3 s, a three-phase diode rectifier of 20 kW is added to the system, and the SAPF can still track the abrupt load current quickly.

After about one fundamental period, the system reaches stability. It shows that the proposed control strategy has good dynamic performance.

In order to further verify the effectiveness of the proposed strategy, a SAPF prototype of 15 kVA is built. The main control chip is TMS320F28335 of TI company. PM50RL1B120 produced by Mitsubshi is used as power devices of the main circuit. In the process of prototype testing, the experimental waveform is recorded by the DPO3014 digital fluorescence oscilloscope produced by the Tektronix Inc in the United States, and the harmonic data are recorded by PM3000A Power Quality Analyzer produced by Voltech Inc. Experimental setups of SAPF are shown as Figure 20. The experimental parameters are as follows:
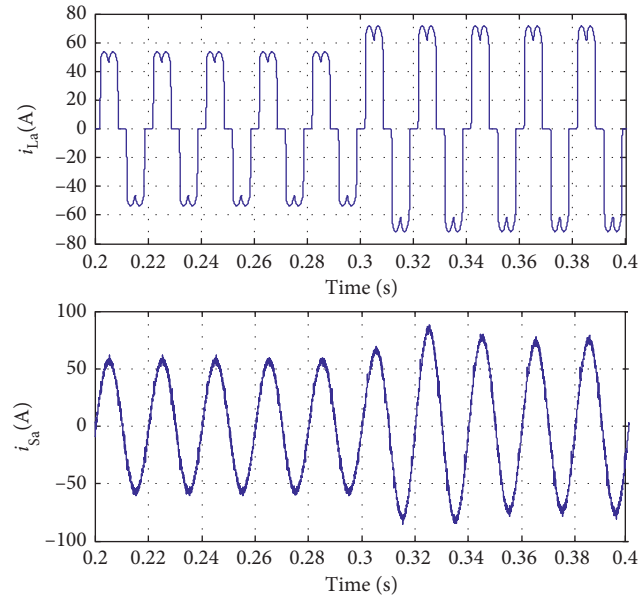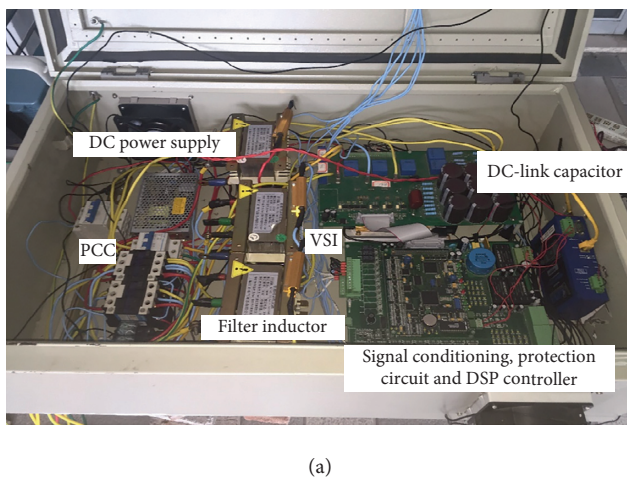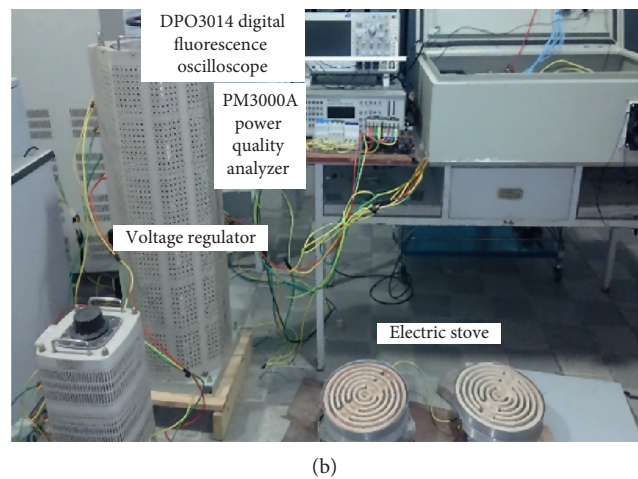
FIGURE 19: Waveforms of load current and source current in the case of abrupt loading.

(a)

(b)

FIGURE 20: Experimental setups of SAPF.

(i) Three-phase source voltage: $U_N = 380$ V and $f = 50$ Hz

(ii) Nonlinear load: two-way three-phase diode rectifier with two series two parallel(2S2P) electric stoves of 5 kW in DC link and a three-phase voltage regulator with a rated power of 15 kVA, rated voltage p of 380 V, and output voltage of 220 V in AC link

(iii) Switching frequency of IGBT: 10 kHz

(iv) Voltage controller parameters: ratio coefficient $K_p = 0.1$ and integral coefficient $K_i = 10$

(v) Current controller parameters: $K_{p0} = 0.5$, $K_i = 160$, $K_{p6} = 0.2$, $K_{i6} = 200$, $K_{p12} = 0.2$, $K_{i12} = 200$, $K_{p18} = 0.5$, $K_{i18} = 200$, and so on

(vi) Other experimental parameters: the parameters including DC-link voltage, DC link capacitance, and

filter inductance are consistent to the simulation parameters

Experimental steady waves using PI controller and PI + multi-VR controllers are shown in Figures 21 and 22. Waveform 2 represents load current, THD of which is 26.1%. Waveform 4 in Figures 21 and 22 represent source current after compensation based on PI controller and PI + multi-VR controllers. Evidently, both of source currents approach nearly sinusoidal by SAPF. However from Table 2, the THD of the source current reduces from 7.34% to 2.86% by using the proposed control strategy. The above results show that the proposed control strategy has good steady performance and control accuracy.

Experimental dynamic results are shown in Figure 23. Before the time of 0.04 s, the SAPF has been invested in the system to finish the harmonic current detection. Besides, voltage controller has been working steadily and DC-link
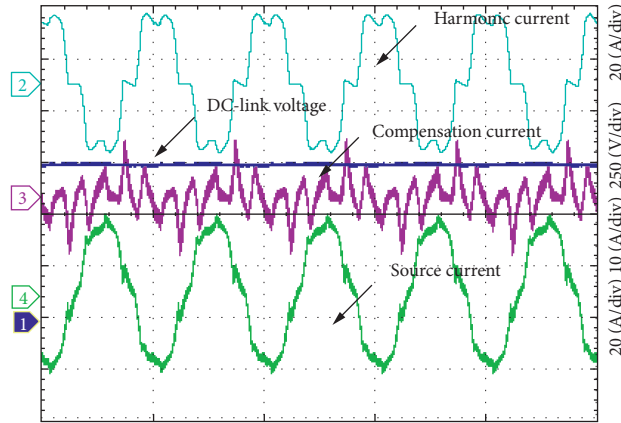
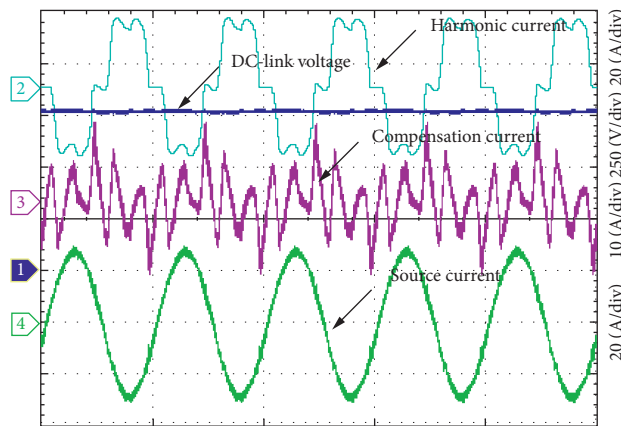FIGURE 21: Experimental steady waves using PI controller.

FIGURE 22: Experimental steady waves for proposed scheme.

TABLE 2: Compensation results with two control algorithms.

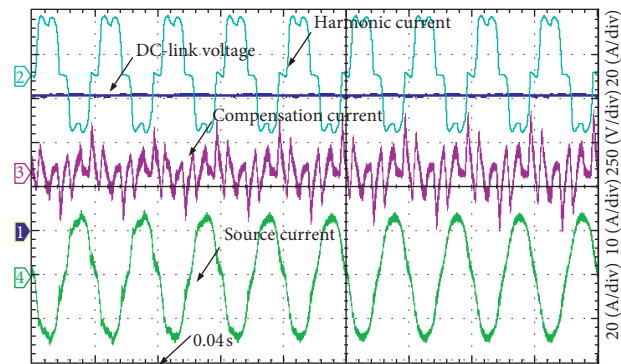| Order of harmonic		5	7	11	13	17	19	THD (%)
Harmonic distortion before compensation (%)		21.3	9.87	5.60	3.36	1.80	0.92	26.1
Harmonic distortion after compensation (%)	With PI controller	2.16	1.86	1.76	1.80	1.74	1.82	7.34
	With the proposed method	0.72	0.48	0.35	0.2	0.18	0.10	2.86

FIGURE 23: Experimental dynamic waveform after adding VR controller.

voltage has been stabilized at 750 V. Moreover, the basic control loop of current controller or PI control has also been run. At the time of 0.04 s, the multi-VR controllers start running. After about 3 fundamental periods, the system enters the new steady state. Experimental results show that the proposed strategy also has good dynamic performance.

6. Conclusion

With development of power electronic technology, a large number of power electronic devices are integrated into the power grid, which causes the harmonic pollution. Through the study on SAPF mathematical model and the principle of VR controller, a current control strategy based on PI and multi-VR controller is proposed in this paper. Through detailed analysis on frequency response characteristic of current closed loop, in that the PI and VR controller can compensate the harmonic currents with zero steady-state error, little phase delay and good dynamic performance are proved. In addition, under the synchronous reference frame, the proposed method is simple enough to compensate the harmonic, which reduces the computation and is better adapted to frequency fluctuation. The simulation and experimental results show that the proposed control strategy is correct and effective, which improves the power quality.

Data Availability

The data used to support the findings of this study are available from the corresponding author upon request.

Conflicts of Interest

The authors declare that there are no conflicts of interest regarding the publication of this paper.

Acknowledgments

References

[1] Q. Zhong, J. Feng, G. Wang, and H. Li, "Feedforward harmonic mitigation strategy for single-phase voltage source converter," *Journal of Electrical and Computer Engineering*, vol. 2018, Article ID 5909346, 10 pages, 2018.

[2] C. Burgos-Mellado, C. Hernandez, R. Cardenas-Dobson et al., "Experimental evaluation of a CPT-based 4-leg active power compensator for distributed generation," *IEEE Journal of Emerging & Selected Topics in Power Electronics*, vol. 5, no. 2, pp. 747–759, 2017.

[3] S. Pettersson, M. Salo, and H. Tuusa, "Applying an LCL-filter to a four-wire active power filter," in *Proceedings of Power Electronics Specialists Conference (PESC'06)*, pp. 1–7, Jeju, South Korea, June 2006.

[4] E. Uz-Logoglu, O. Salor, and M. Ermis, "Real-time detection of interharmonics and harmonics of AC electric arc furnaces on GPU framework," in *Proceedings of IEEE Industry Applications Society Meeting (IAS'17)*, pp. 1–8, Cincinnati, OH, USA, October 2017.

[5] S. Rahmani, A. Hamadi, K. Al-Haddad, and L. A. Dessaint, "A combination of shunt hybrid power filter and thyristor-controlled reactor for power quality," *IEEE Transactions on Industrial Electronics*, vol. 61, no. 5, pp. 2152–2164, 2014.

[6] S. M. M. Gazafrudi, A. T. Langerudy, E. F. Fuchs et al., "Power quality issues in railway electrification: a comprehensive perspective," *IEEE Transactions on Industrial Electronics*, vol. 62, no. 5, pp. 3081–3090, 2015.

[7] M. K. M. Valappil and M. K. Mishra, "Three-leg inverter-based distribution static compensator topology for compensating unbalanced and non-linear loads," *IET Power Electronics*, vol. 8, no. 11, pp. 2076–2084, 2015.

[8] L. Wang, C. S. Lam, M. C. Wong, N.-Y. Dai, K.-W. Lao, and C. K. Wong, "Non-linear adaptive hysteresis band pulse-width modulation control for hybrid active power filters to reduce switching loss," *IET Power Electronics*, vol. 8, no. 11, pp. 2156–2167, 2015.

[9] S. Q. Zhang, D. Ke, B. Xie, and Y. Kang, "Selective harmonic current control based on multiple synchronous rotating coordinates," *Proceedings of the CSEE*, vol. 30, no. 3, pp. 55–62, 2010.

[10] A. D. Aquila, M. Liserre, V. G. Monopoli et al., "Overview of PI-based solutions for the control of DC buses of a single-phase H-bridge multilevel active rectifier," *IEEE Transactions on Industry Applications*, vol. 44, no. 3, pp. 857–866, 2008.

[11] Z. Chelli, R. Toufouti, A. Omeiri, and S. Saad, "Hysteresis control for shunt active power filter under unbalanced three phase load conditions," *Journal of Electrical and Computer Engineering*, vol. 2015, Article ID 391040, 9 pages, 2015.

[12] Y.-H. Kim, J.-G. Kim, Y.-H. Ji, C.-Y. Won, and Y.-C. Jung, "Photovoltaic parallel resonant dc-link soft switching inverter using hysteresis current control," in *Proceedings of the Applied Power Electronics Conference and Exposition (APEC'10)*, pp. 2275–2280, Palm Springs, CA, USA, February 2010.

[13] Z. X. Zou, K. Zhou, Z. Wang, and M. Cheng, "Frequency-adaptive fractional-order repetitive control of shunt active power filters," *IEEE Transactions on Industrial Electronics*, vol. 62, no. 3, pp. 1659–1668, 2015.

[14] Y. Wang, H. Zheng, R. Wang et al., "A novel control scheme based on the synchronous frame for APF," *Journal of Power Electronics*, vol. 17, 2017.

[15] W. Jiang, L. Wang, W. Ma et al., "A control method based on current tracking error compensation of deadbeat control for a three-phase active power filter," *Proceedings of the CSEE*, vol. 36, no. 20, pp. 5605–5615, 2016.

[16] S. Buso, T. Caldognetto, and D. I. Brandao, "Dead-beat current controller for voltage-source converters with improved large-signal response," *IEEE Transactions on Industry Applications*, vol. 52, no. 2, pp. 1588–1596, 2016.

[17] L. Herman, I. Papic, and B. Blazic, "A proportional-resonant current controller for selective harmonic compensation in a hybrid active power filter," *IEEE Transactions on Power Delivery*, vol. 29, no. 5, pp. 2055–2065, 2014.

[18] J. B. Hu, Y. K. He, H. S. Wang et al., "Proportional-resonant current control scheme for rotor-side converter of doubly-fed induction generators under unbalanced network voltage conditions," *Proceedings of the CSEE*, vol. 30, no. 6, pp. 48–56, 2010.

[19] B. Singh, S. K. Dube, and S. R. Arya, "An improved control algorithm of DSTATCOM for power quality improvement," *International Journal of Electrical Power & Energy Systems*, vol. 64, no. 64, pp. 493–504, 2015.

[20] H. Yi, F. Zhuo, Y. Zhang et al., "A source-current-detected shunt active power filter control scheme based on vector resonant controller," *IEEE Transactions on Industry Applications*, vol. 50, no. 3, pp. 1953–1965, 2014.

[21] A. Szromba, "Conductance-controlled global compensation type shunt active power filter," *Archives of Electrical Engineering*, vol. 64, no. 2, pp. 259–274, 2015.

[22] X. U. Hailiang, Z. Liao, and H. E. Yikang, "Key points of proportional-resonant controller applied for PWM converters," *Automation of Electric Power Systems*, vol. 39, no. 18, pp. 151–159, 2015.